This article has been accepted for publication in a future issue of this journal, but has not been fully edited. Content may change prior to final publication. Citation information: DOI 10.1109/OJIA.2020.3035851, IEEE Open Journal of Industry Applications

A V2G Integrated Battery Charger based on an Open End Winding Multilevel Configuration

S. Foti, *Member, IEEE,* A. Testa, *Member, IEEE,* G. Scelba, *Senior Member, IEEE,* S. De Caro, *Member, IEEE,* L. D. Tornello, *Student Member, IEEE*

Abstract A new approach to obtain an integrated battery charger is described in this paper, based on the Asymmetrical Hybrid Multilevel Converter topology. Such a particular open-end winding motor configuration, which has proved to be more efficient than conventional inverter topologies in EV motor drive applications, can be turned in an on-board battery charger only by acting on the control system. Thus, no circuit reconfiguration through electro-mechanical switches is required. Moreover, by introducing a single extra power switch, a bilateral power flow can be managed enabling vehicle to grid operations. The obtained integrated battery charger can be supplied either by a standard ac single-phase grid, either by a dc power source for direct connection to domestic energy resources. The proposed approach enables a new remarkable function to the asymmetrical hybrid multilevel converter at a marginal extra cost, thus mitigating the larger complexity and cost of such an inverter if compared with conventional topologies.

***Index Terms*—Multilevel power converter, battery charger, electric vehicles, DC-DC power conversion, DC-AC power conversion.**

I. Introduction

ELECTRIC vehicles (EV) have gained a great interest over the last decade as a mean to reduce the air pollution in urban areas and the global warming. Moreover, EV are today mayor players of the energy transition towards Renewable Energy Sources (RES), providing the ground for exploiting RES in transportation. EV can only rely on external power sources for charging the batteries, making the Battery Charger (BC) an element of major concerning. Based on power ratings, the battery charger may be classified in slow (up to 3.7 kW), quick (from 3.7 to 22 kW) or fast (over 22 kW). BCs can be also grouped in On-board Battery Chargers (OBC) and stand-alone, or off-board, systems. The first group encompasses ac single-phase systems for slow charge, or three-phase systems for quick charge. These devices are on-board installed and require only a minimum external equipment [1]-[9]. Fast dc chargers, rated up to 200 kW, are instead bulky wall mounted systems, powered by a three-phase grid, or by a suitable energy storage system. Conventional OBC are unidirectional devices, managing a power stream from the power source to the batteries. However, using bidirectional battery chargers, EV may provide new tools to cope with the intermittent production of RES based generation plants. In fact, according to the Vehicle to Home (V2H) and Vehicle to Building (V2B) principles, bidirectional chargers could manage the batteries of parked EV to optimize the energy demand on residential or commercial scale, often in conjunction with controllable loads. Moreover, by remotely controlling bidirectional chargers, it is possible to turn parked EV into components of distributed energy storage systems, managed to draw power from the grid during peak of renewable energy production, and to supply electricity to the grid when the demand rises. Vehicle to Grid (V2G) allows electricity grid operators to reduce investments in energy storage systems necessary to cope with the intermittent nature of RES, and, vehicle owners to obtain additional revenues for the services provided to the grid. OBC are generally based on a two-stage configuration [10], [11]; the first stage performs the ac-dc conversion with near-unity power factor, whereas the second one controlling the battery voltage and current. The simplest ac-dc stage is made of an inexpensive diode rectifier, which, however, would require a bulky inductive input filter to cope with distortion of the grid current. Hence, a dc-dc boost converter is generally added to the diode rectifier, in order to accomplish an active power factor correction. Moreover, bidirectional energy flows are made possible by exploiting bidirectional buck-boost converters and PWM rectifiers. The dc-dc stage is generally realized around a bridge converter. Although effective, the two-stage configuration is burdened by a high part count, a low power density and a low efficiency. Simpler single-stage configurations have been also proposed [12], which however feature a lower degree of flexibility and require a more complex control. In fact, a single converter is tasked to deal at a time either with the PF control on the ac side, either with control of the voltage and current on the dc side. Moreover, both two-stage and single-stage OBCs require a quite large output filter, composed of a dc bus capacitor and an inductor, in order to suitably reduce the battery current ripple [13]-[14].

S. Foti, A. Testa and S. De Caro are with the Department of Engineering, University of Messina, C/da di Dio (S. Agata), 98166 Messina, Italy (e-mail: sfoti@unime.it).
G. Scelba and L. D. Tornello are with the Department of Electrical, Electronics and Computer Engineering, University of Catania, Viale Andrea Doria 6, 95125 Catania, Italy (e-mail: giacomo.scelba@unict.it).

This work is licensed under a Creative Commons Attribution 4.0 License. For more information, see https://creativecommons.org/licenses/by/4.0/

This article has been accepted for publication in a future issue of this journal, but has not been fully edited. Content may change prior to final publication. Citation information: DOI 10.1109/OJIA.2020.3035851, IEEE Open Journal of Industry Applications

Being located on board, OBC has a negative impact on EV range, available internal space and maximum payload. These disadvantages can be mitigated by adopting the Integrated Battery Charger (IBC) approach. Since the propulsion drive is inactive when recharging the battery from the grid, some components of the power train such as the motor windings and some parts of the inverter can be shared with the BC, as shown in Fig. 1, thus reducing the amount of additional components, as well as, the weight and space required [6].

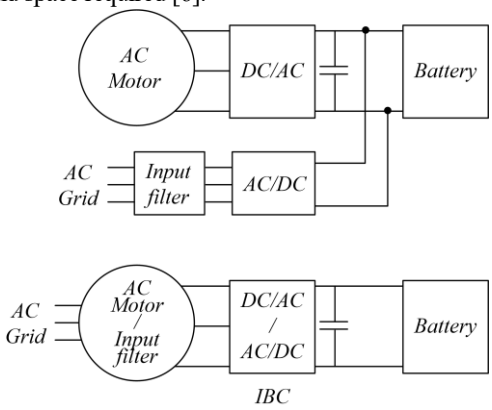

Fig. 1. Schematic of a conventional OBC (top) and of an IBC (down).

Reconfigurable Voltage Source Inverter (VSI) have been proposed in the past literature, which can be turned in dc-dc converters for battery charging [7], [15], [16]. Only a partial integration is however obtained, as some additional components, such as the rectifier, the inductor, or some extra switches are required. OBC based on reconfiguration of Multilevel Inverters (MLI) have been also proposed, featuring different levels of integration [17], [18] and an Open-end Winding (OW) configuration is pioneered in [19]. However, the last is a very special kind of integrated battery charger as it only allows to charge a secondary battery from the main one via the motor, in a vehicle with two isolated dc buses; therefore, a conventional main battery charger is anyway required. A bidirectional OBC has been also proposed using an eight-switch inverter, followed by an interleaved dc-dc converter suitable for Vehicle to Grid (V2G) and Grid to Vehicle (G2V) operations [20].

This paper describes a new approach for realizing an integrated bidirectional battery charger exploiting an asymmetrical OW topology, the Asymmetrical Hybrid Multilevel Converter (AHMC), which has been recently proposed as an alternative to conventional inverters for ac motor drives [21]-[27]. As shown in Fig. 2, it features an OW ac machine fed by a Neutral Point Clamped (NPC) multilevel inverter (MLI) from one side and a conventional PWM Two-level Inverter (TLI) from the other side. The main NPC inverter is low frequency operated, while the TLI acts as an active power filter. In the following, it is demonstrated that an AHMC can be turned in an on-board battery charger barely acting on the control system. This inexpensively gives a valuable extra function to the asymmetrical OW topology, only achievable at the cost of additional circuitry on conventional topologies. Furthermore, by adding a single extra bidirectional switch, a bidirectional power flow can be managed, making the proposed solution also suitable for V2G applications. Such an extra switch will likely become unnecessary on next generation EV, where the battery voltage will be raised up to *800V*, making no longer required a voltage step-up in V2G mode. Finally, the proposed system can be also connected to a dc power source, enabling a direct connection of the battery to PV plants, or distributed energy storage systems, for V2H or V2B applications.

II. Traction Mode

According to the basic AHMC configuration of Fig. 2, the TLI is tasked to supply only reactive power to the OW machine. Hence, it can be supplied through a floating capacitor making a second independent power source unnecessary. A couple of diodes and an additional bidirectional power switch are added to the basic AHMC structure to enable G2V and V2G operations.

In Traction Mode (TM), the power sockets of the battery charger are disconnected from power plugs and diodes D_{T1} and D_{T2} are reverse polarized, while the bidirectional switch S_g is turned *off*. The MLI j-phase output voltage V_{jMLI}, which is the voltage between the terminal *j* and the mid-point n' of the DC bus, is given by:

$$V_{jMLI} = \frac{l'-1}{2} V_{DC}' \qquad l' = 0,1,2 \tag{1}$$

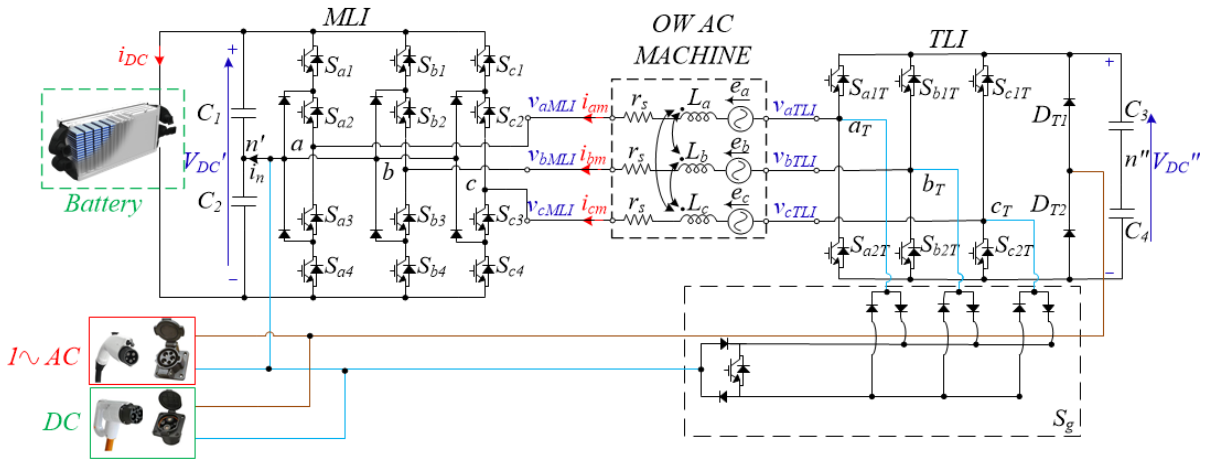

Fig.2. MLI+TLI AHMC topology

This work is licensed under a Creative Commons Attribution 4.0 License. For more information, see https://creativecommons.org/licenses/by/4.0/

This article has been accepted for publication in a future issue of this journal, but has not been fully edited. Content may change prior to final publication. Citation information: DOI 10.1109/OJIA.2020.3035851, IEEE Open Journal of Industry Applications

being, V_{DC}' the total battery voltage. This leads to three different output voltage levels, namely: $-V_{DC}'/2$, $V_{DC}'/2$ and 0, according to the rectifier j-pole state l'. The voltage between the TLI *j*-phase output terminal j_T and the mid-point n" of the TLI dc-bus is given by:

$$V_{jTLI} = \frac{2l''-1}{2} V_{DC}'' \qquad l''=0,1 \tag{2}$$

leading to two voltage levels, namely: $-V_{DC}''/2$ and $V_{DC}''/2$, according to the inverter j-pole state l''.

The TLI is supplied through a flying capacitor in order to prevent the circulation of zero sequence currents. Hence, the two converters are connected to two independent voltage sources, V_{DC}' and V_{DC}'' and the voltage V_{jm} across the open-end phase winding j, can be expressed as:

$$V_{jm} = \frac{l'-1}{2} V_{DC}' - \frac{(2l''-1)}{2} V_{DC}'' - V_{n'n''} \quad l'=0,1,2 \quad l''=0,1 \tag{3}$$

being $V_{n'n''}$ the voltage between the mid points n' and n'' of the dc-buses of the two converters, which is given by:

$$V_{n'n''} = \frac{1}{3}(V_{aMLI}+V_{bMLI}+V_{cMLI}) - \frac{1}{3}(V_{aTLI}+V_{bTLI}+V_{cTLI}) \tag{4}$$

The MLI+TLI converter of Fig. 2 features only twelve power switches, but is equivalent to a six-level NPC, or Flying Capacitor (FC) inverter encompassing thirty power switches [21]. Moreover, a three-level staircase voltage modulation technique is used in motoring mode on the MLI, in order to reduce the switching losses, while a high-frequency PWM is exploited on the TLI side to accurately shape the motor current.

As a result, the apparent switching frequency of the whole system is equal to that of the TLI, although the MLI which processes the power delivered to the machine switches at the fundamental frequency. Hence, compared to conventional PWM operated MLI, the proposed solution generates lower conversion power losses [19].

A specific current control strategy has been developed to manage the AHMC in motoring mode. As shown in Fig. 3, it encompasses two systems, respectively managing the MLI and the TLI [22]. The MLI current control system acts predictively on the fundamental component of the MLI output voltage. The reference stator voltage magnitude $|V_{1MLI}^*|$ is first computed from a mathematical model of the motor then devices switching times are obtained through a step modulator.

The TLI control is tasked to accomplish four tasks:

- Predictively cancels the stator voltage harmonics caused by MLI step modulation, as shown in Fig. 4;
- Implementation of the current closed-loop control in a synchronous reference frame d,q;
- Implementation of the TLI dc-bus voltage closed-loop control;
- cope with voltage unbalance between MLI dc-bus capacitors, by managing the current entering in the node n'.

The auxiliary inverter voltage reference V^*_{jTLI} is obtained as the sum of four different terms. The first contribution, named hereinafter as V_{jh}, is computed to compensate low-order harmonics components generated by MLI. In fact, the staircase MLI phase voltage V_{jMLI}, consists of the fundamental component V_{j1MLI} and an infinite number of harmonics V_{jh} of odd order.

$$V_{jMLI} = V_{j1MLI} + \sum_{h=1,3,5...}^{\infty} V_{jh} \tag{5}$$

Accordingly, the TLI reference voltage term V_{jTLIh} is made equal to V_{jh} which is the difference between the staircase voltage V_{jMLI} and its fundamental harmonic V_{j1MLI}, as displayed in Fig. 4. A further term of the voltage reference V_{jTLI} is generated by the phase currents control system, Fig. 3. This is based on a current control approach exploiting two PI regulators, whose outputs are processed to compute the second term V^*_{TLIr} of the TLI voltage reference. Two additional key functions are required by the considered topology dealing with control of the voltage V_{DC}'' of the TLI DC-Bus floating capacitor and equalization of the voltages across the MLI DC-bus capacitors. Theoretically, a null average power is exchanged between the TLI and the machine; therefore, the DC-bus voltage V_{DC}'' is ideally constant. However, inverter power losses cause a progressive discharge of the TLI DC-bus capacitor, which can be charged only by establishing a controlled active power flow between the two inverters. The power P_P required to keep constant V_{DC}'' is determined by a closed loop controller processing the error between the reference DC bus voltage $V_{DC}''^*$ and the actual value V_{DC}'', as shown in Fig. 3. Two d,q voltage components V_{qCap} and V_{dCap} are then computed in order to force the transfer of the required active power P_p from the MLI to the TLI with a null reactive power exchange. A third term $V^*_{jTLICap}$ of the TLI voltage reference is finally computed by transforming V_{qCap} and V_{dCap} into the stationary *abc* reference frame. The equalization of the voltages across the MLI DC-bus capacitors is obtained by controlling the current i_n entering the mid-point of the MLI DC-bus, as deeply discussed in [22] and [31]. A fourth term of the TLI voltage reference V^*_{jTLIn} is then produced by processing the difference between actual values of the voltages across the two capacitors of the MLI DC-bus. Finally, the TLI reference voltage V^*_{JTLI} is determined as:

$$V^*_{jTLI} = V^*_{jTLIr} + V^*_{jTLIh} + V^*_{jTLIcap} + V^*_{jTLIn.} \tag{6}$$

The start-up of the system has been discussed in [21]. The flying TLI DC Bus is first charged by the capacitor voltage control system, acting on $V^*_{jTLICap}$, while providing a small DC reference voltage to the MLI. Once the DC Bus voltage has reached its reference value, the traction drive is ready to operate. The start-up of the system powering the PMSM of Table 5 is shown in Fig. 5, where $V_{DC}''= V_{DC}'/2$ and $C_1=C_2=C_3=C_4=820\mu F$.

III. AC-DC G2V AND V2G

The AHMC can be connected to a single-phase ac grid for charging the battery by inserting the ac plug in the ac socket, while leaving disconnected the dc socket. Therefore, according to Fig. 2, the grid voltage is applied between the mid-point of the dc bus of the MLI and the mid-point of the two series connected diodes D_{T1} and D_{T2}. The obtained non-isolated IBC satisfies the SAE J1772 standard for conductive chargers, as EV batteries are generally not grounded to chassis for safety and electromagnetic interference issues [29].

This work is licensed under a Creative Commons Attribution 4.0 License. For more information, see https://creativecommons.org/licenses/by/4.0/

This article has been accepted for publication in a future issue of this journal, but has not been fully edited. Content may change prior to final publication. Citation information: DOI 10.1109/OJIA.2020.3035851, IEEE Open Journal of Industry Applications

The standard charging procedure for Lithium-Ion batteries is shown in Fig. 6. It is known as Constant Current – Constant Voltage (CC-CV), because a constant current is provided to the battery until it reaches the maximum charging voltage, then a constant voltage is maintained while the current drops up to 3÷5 percent of the current rating, at which point the battery is considered charged. Cell balancing is accomplished by the internal Battery Management System (BMS).

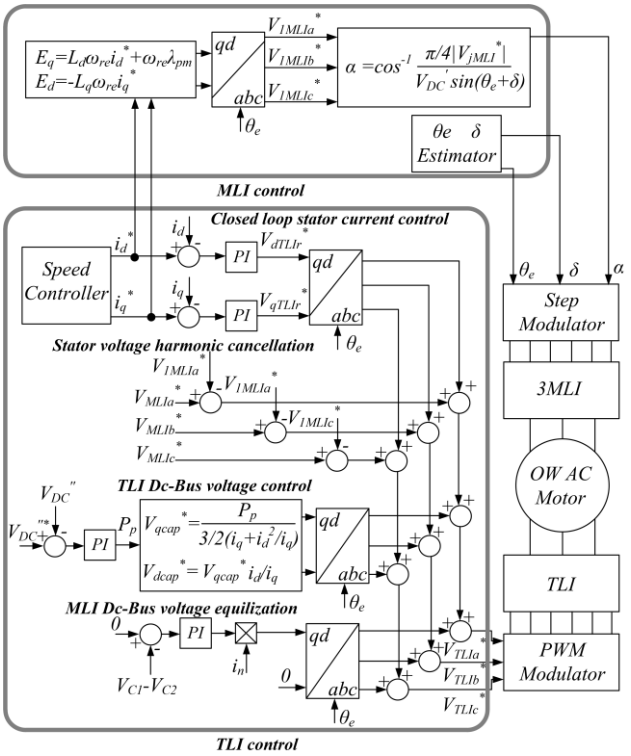

Fig. 3: TM: control scheme.

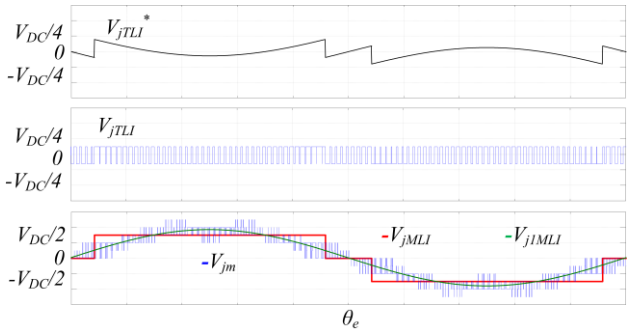

Fig. 4. TM: TLI reference voltage, TLI output voltage and motor voltage.

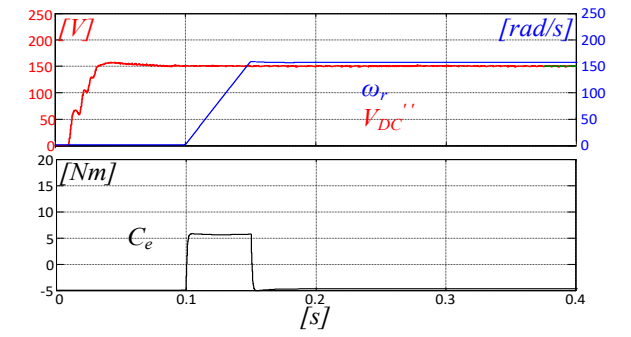

Fig. 5. System start-up in traction mode: ω_r, TLI DC-Bus voltage and torque.

Motor motion when charging the battery may be prevented by a mechanical lock, additional inverters or by avoiding the production of torque. The last approach is adopted by forcing the circulation of only zero-sequence currents through the stator winding of the machine. Thus, the switches of the three legs of both the MLI and TLI are synchronously operated as they belonged to the same phase. As a result, the equivalent single-phase circuit of the system can be considered, as shown in Fig. 7. In G2V mode the system works as a PFC, cyclically switching from a Buck-like configuration ($|V_g|>V_{DC}'/2$) to a Boost-like one ($|V_g|<V_{DC}'/2$), as shown in Fig. 8. The stator winding plays the role of power inductor, while that of output capacitor is played alternatively, by one of the two MLI dc-bus capacitors. In Buck mode, as shown in Fig. 9 and according to Table I, switches S_{j1}, S_{j2}, S_{j3}, S_{j4} and S_g are turned off, while S_{j1T} or S_{j2T} are PWM operated, depending on the sign of the grid voltage, to control the charge current. In Boost mode S_{j1T} and S_{j2T} are turned on and the battery current is managed through S_{j2} or S_{j3}, according to the sign of the grid voltage.

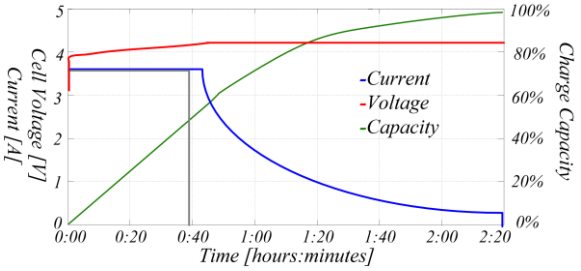

Fig. 6. Li-Ion battery charging diagram.

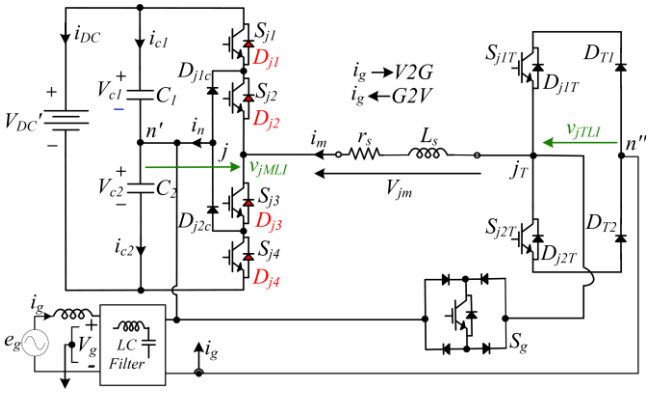

Fig. 7: AHMC connected to a single-phase ac grid.

The phase current is managed through a hysteresis controller, which drives S_{j1T} or S_{j2T} in Buck mode and S_{j2} or S_{j3} in Boost mode. Unlike conventional Buck PFC, no hold-up issues for the output capacitor arise, because, the power transfer takes place along an entire half-period of the grid voltage. No extra current sensors are required, because those normally already present in an EV propulsion drive can be used. According to Table I, only a single switch per phase is PWM operated at a time, leading to low power losses.

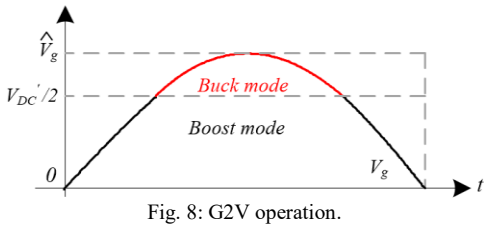

Fig. 8: G2V operation.

This work is licensed under a Creative Commons Attribution 4.0 License. For more information, see https://creativecommons.org/licenses/by/4.0/

This article has been accepted for publication in a future issue of this journal, but has not been fully edited. Content may change prior to final publication. Citation information: DOI 10.1109/OJIA.2020.3035851, IEEE Open Journal of Industry Applications

As shown in Fig. 10, the reference grid current i_g^* is a sinusoidal signal synchronized with the grid voltage, whose magnitude is given by a PI controller processing the battery voltage, or current, error. The ratio of V_g to its peak value is computed to determine the sign of the grid reference current. Figure 11 deals with the transient taking place when switching from constant current to constant voltage control. Current and voltage peaks can be managed by properly tuning voltage and current regulators.

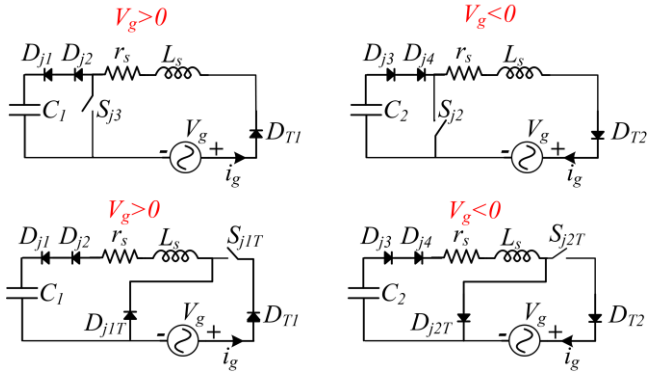

Fig. 9: G2V ac-dc operation: Boost (up) and Buck(down) modes.

Table I – G2V ac-dc operation: switching table.

G2V		MLI				TLI		
		S_{j1}	S_{j2}	S_{j3}	S_{j4}	S_{j1T}	S_{j2T}	S_g
Buck	$V_g>0$	off	off	off	off	PWM	off	off
$\|V_g\|>V_{DC}'/2$	$V_g<0$	off	off	off	off	off	PWM	off
Boost	$V_g>0$	off	off	PWM	off	on	off	off
$\|V_g\|<V_{DC}'/2$	$V_g<0$	off	PWM	off	off	off	on	off

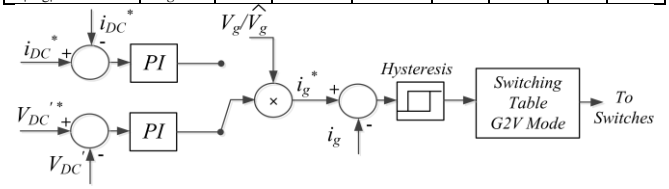

Fig. 10. G2V ac-dc control scheme.

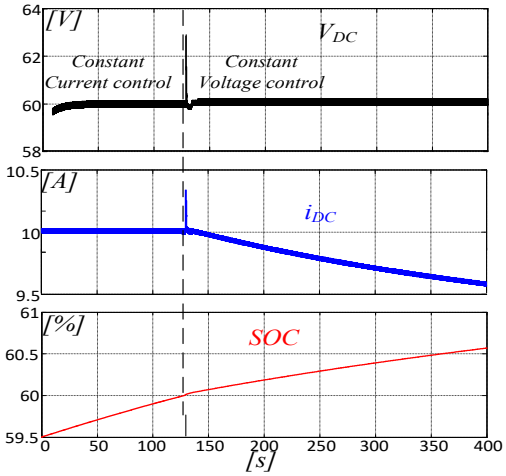

Fig. 11. Switching from constant current to constant voltage charging mode.

A battery voltage ripple at twice the grid frequency is generated, mitigated by the MLI dc-bus capacitance, which is given by the series connection of C_1 and C_2. However, in ac single-phase G2V operation only one out of C_1 and C_2 is powered at a time. Hence, the ac-dc converter output capacitance is twice the total MLI dc bus capacitance. The minimum dc-bus capacitance required to obtain a given residual battery voltage ripple $\Delta V_{DC}\%$ is given by [30]:

$$C_{DC\min} = \frac{P_{DCn}}{4V_{DCn}^2 f_e \Delta V_{DC\%}} 100 \tag{7}$$

In Fig. 12 the minimum capacitance C_{DC10} required to obtain a 10% ripple is plotted as function of the battery voltage. Achieved results well cope with dc bus capacitance of EV traction drives, which ranges from *200* to *2000* μF.

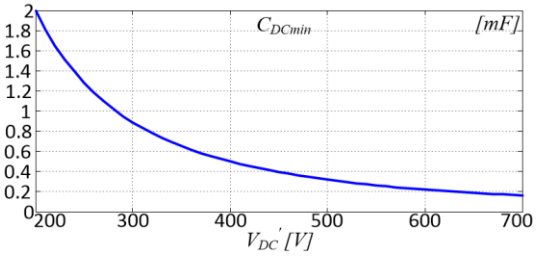

Fig. 12: C_{DC10} vs V_{DC}' (V_g=240V, P_{DCN}=3kW, f_e=50Hz).

Battery current ripple at the switching frequency is function of the stator winding inductance [30]; the minimum inductance required to achieve a given current ripple $\Delta i_{DC\%}$ is:

$$\textit{Boost mode}\quad L_{s\min} = \frac{V_{DCn}^2}{4P_{DCn} f_{sw} \Delta i_{DC\%}} 100 \tag{8}$$

$$\textit{Buck mode}\quad L_{s\min} = \frac{V_{DCn}^2}{4P_{DCn} f_{sw} \Delta i_{DC\%}} \left(1 - \frac{V_{DCn}}{2V_g}\right) 100 \tag{9}$$

The minimum inductance L_{S10} required to achieve a *10%* current ripple is plotted in Fig. 13 as function of the switching frequency and battery voltage. Obtained values well match the typical range of the stator inductance of EV motors (*50÷400 mH*).

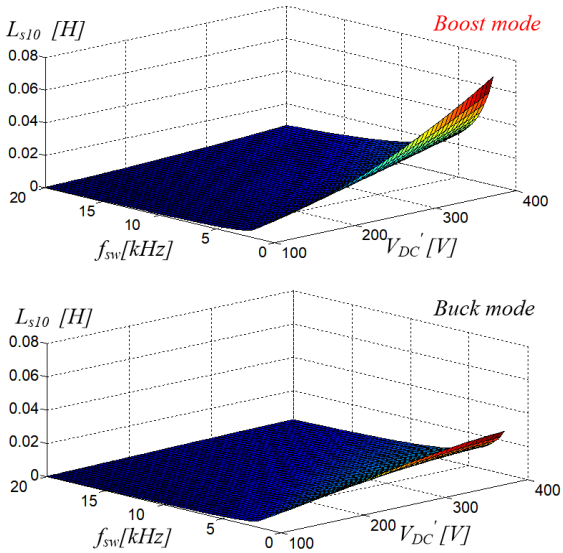

Fig. 13: L_{s10} (V_g=240V, V_{DCN}=350V)

V2G deals with remotely managed power transfer from the battery to the grid. As shown in Fig. 14, a voltage step-up

This work is licensed under a Creative Commons Attribution 4.0 License. For more information, see https://creativecommons.org/licenses/by/4.0/

This article has been accepted for publication in a future issue of this journal, but has not been fully edited. Content may change prior to final publication. Citation information: DOI 10.1109/OJIA.2020.3035851, IEEE Open Journal of Industry Applications

capability is required to cope with common battery (*300-400V*) and ac grid (*110-240V*) voltage levels, which is provided through the introduction of the additional switch S_g. However, on the next generation EV the battery voltage will be increased up to *800V*, this will make no longer necessary a voltage step-up in V2G mode, thus eliminating the need for the additional switch S_g. According to Fig. 15 and Table II, only a single switch is PWM operated at a time in V2G mode; in particular, S_{j1} or S_{j4} are operated in Buck mode, and S_g in Boost mode. The battery current control scheme in V2G dc-ac mode is shown in Fig. 16. No additional voltage sensors are required because exploiting those already used for motor drive control.

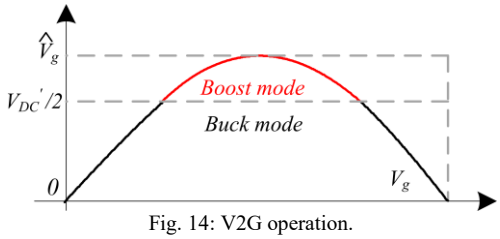

Fig. 14: V2G operation.

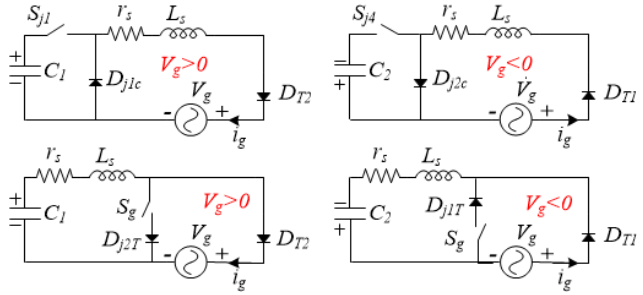

Fig. 15: V2G dc-ac operation: Buck (up) and Boost (down) modes.

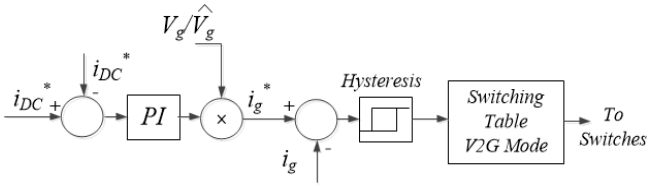

Fig. 16: V2G dc-ac control scheme.

Table II – V2G dc-ac operation: switching table.

V2G		MLI				TLI		
		S_{j1}	S_{j2}	S_{j3}	S_{j4}	S_{j1T}	S_{j2T}	S_g
Buck	$V_g>0$	PWM	on	off	off	off	on	off
$\|V_g\|<V_{DC}'/2$	$V_g<0$	off	off	on	PWM	on	off	off
Boost	$V_g>0$	on	on	off	off	off	on	PWM
$\|V_g\|>V_{DC}'/2$	$V_g<0$	off	off	on	on	on	off	PWM

IV. DC-DC G2V AND V2G

According to the V2H and V2B concepts, EV batteries can be exploited to store energy in order to increase the capability of local energy storage systems and to provide backup power [4]. In residential and commercial buildings EV can be connected to power sources and loads by a conventional ac grid, or by a purposely realized dc power system. The first solution is inexpensive although requiring more power processing steps. In fact, the majority of loads and energy storage systems require a dc supply, while power source produce a dc voltage. Hence, a direct dc connection is more efficient, avoiding lossy ac-dc and dc-ac conversions. This however requires a dc power system, as those today used in data centers and telecommunication systems, which will likely become common in next years also in the residential sector [29]. The AHMC topology may be easily turned into a bidirectional IBC connected to a dc grid by inserting the dc plug in the dc socket. The dc grid is thus connected between the mid-point of the dc bus of the MLI and the mid-point of the two series connected diodes D_{T1} and D_{T2}, as shown in Fig. 17. In G2V dc-dc operation only the capacitor C_1 is powered, thus its voltage V_{C1} reaches the battery voltage V_{DC}', while V_{C2} drops until zero, therefore, differently from what happens in ac-dc G2V operation, the converter output voltage is the full battery voltage. The converter may charge the battery working as a Buck converter (when $V_g>V_{DC}'$) or as a Boost one (when $V_g<V_{DC}$), as shown in Fig. 18 and according to Table III. The battery current control scheme in G2V dc-dc mode is shown in Fig. 19.

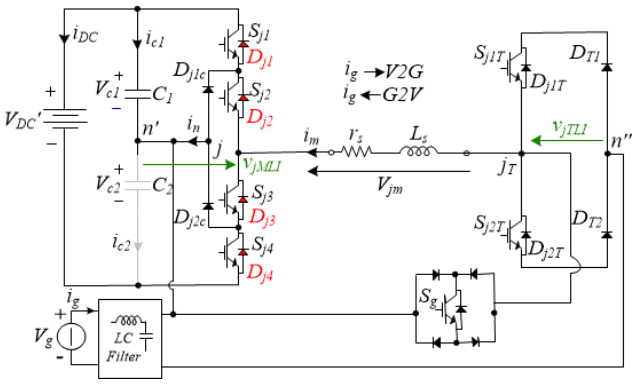

Fig. 17: AHMC connected to a dc grid.

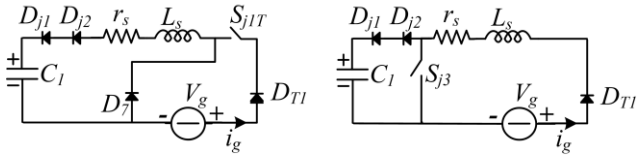

Fig. 18: G2V dc-dc operation: Buck (left) and Boost (right) modes.

Table III – G2V dc-dc operation: switching table.

G2V		MLI				TLI		
		S_{j1}	S_{j2}	S_{j3}	S_{j4}	S_{j1T}	S_{j2T}	S_g
Buck	$\|V_g\|>V_{DC}'$	off	off	off	off	PWM	off	off
Boost	$\|V_g\|<V_{DC}'$	off	off	PWM	off	on	off	off

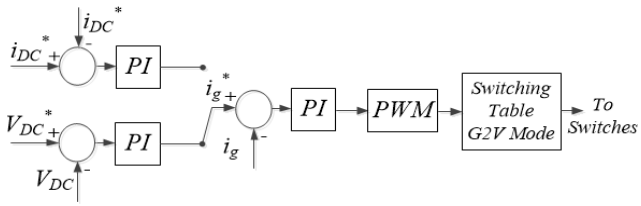

Fig. 19: G2V dc-dc control scheme.

Battery current ripple at the switching frequency is related to the stator winding inductance L_S by:

Buck mode
$$\Delta i_b = \frac{V_g(1-D)DT_s}{f_{sw}L_s} \tag{10}$$

This work is licensed under a Creative Commons Attribution 4.0 License. For more information, see https://creativecommons.org/licenses/by/4.0/

This article has been accepted for publication in a future issue of this journal, but has not been fully edited. Content may change prior to final publication. Citation information: DOI 10.1109/OJIA.2020.3035851, IEEE Open Journal of Industry Applications

$$\textit{Boost mode} \qquad \Delta i_b = \frac{V_g D}{f_{sw} L_s} \tag{11}$$

The maximum amplitude of the current ripple occurs in Boost mode at $D=1$ and $V_g=\hat{V}_g$, hence, the minimum inductance required to achieve a given current ripple $\Delta i_{DC\%}$ is:

$$L_{s\,\min} = \frac{V_g V_{DCn}}{4 P_{DCn} f_{sw} \Delta i_{DC\%}} 100 \tag{12}$$

The minimum inductance L_{SI0} required to achieve a *10%* of current ripple is plotted in Fig. 20.

The AHMC can also accomplish V2G dc-dc operation. The converter input voltage is in this case the battery voltage, being V_{C2} null. The system may work as a Buck converter (when $V_g<V_{DC}'$) or as a Boost one (when $V_g>V_{DC}$), as shown in Fig. 21 and according to Table IV. No standard voltage levels have been yet defined for domestic dc microgrids and different voltages are today considered, ranging from *48V* to *380V*, while, the voltage of battery packs today ranges from *300V* to *400V* and higher levels, up to *800V*, are envisaged in next years. Thus, voltage step-up capability is in most cases unnecessary. The battery current control scheme in V2G dc-dc mode is shown in Fig. 22.

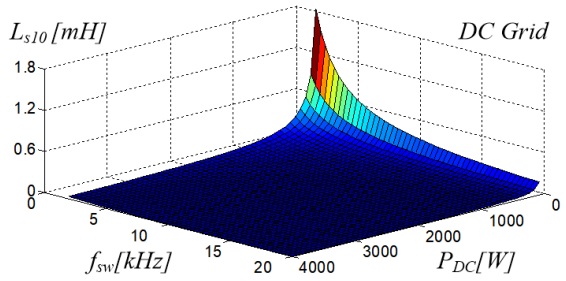

Fig. 20: L_{s10} versus P_{DC} and f_{sw} ($V_g=240V$, $V_{DC}'=350V$)

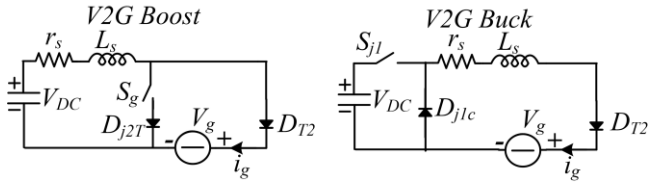

Fig. 21: V2G operation: Buck and Boost modes.

Table IV – V2G dc-dc operation: switching table.

V2G		MLI				TLI		
		S_{j1}	S_{j2}	S_{j3}	S_{j4}	S_{j1T}	S_{j2T}	S_g
Buck	$\|V_g\|>V_{DC}'$	PWM	on	off	off	off	on	off
Boost	$\|V_g\|<V_{DC}'$	on	on	off	off	off	on	PWM

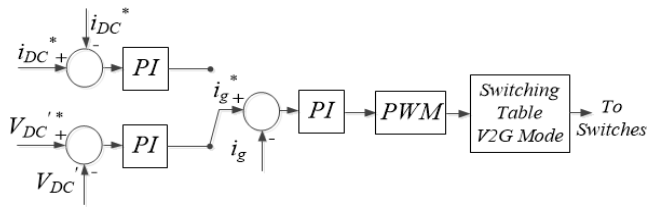

Fig. 22: V2G dc-dc control scheme.

V. Performance Evaluation

Experimental tests have been performed in order to assess the performance of the proposed topology in traction, G2V and V2G modes. As shown in Fig. 23, a six-level IGBT AHMC composed by three-level NPC inverter and a TLI feeding a *2kW* Open-end Winding Permanent Magnet Synchronous Motors was used, whose parameters are listed in Table V. The control was implemented in a dSPACE DS1006 board. The system has been connected on one side to *4×15V, 20Ah* Lithium-Ion battery pack and on the other side to a single-phase ac grid ($V_g=110V$, *50Hz*) or to a dc grid (*60V*). A *15kW* Programmable AC Grid Simulator has been adopted to simulate the ac grid while a *1000V-30A* dc power supply has been used to emulate the dc grid. The TLI floating capacitor was *860µF* and $C_1=C_2=820\mu F$. The width of the hysteresis band of the current controller has been experimental adjusted in order to obtain a *10 KHz* average switching frequency. An LCL filter is introduced to mitigate high frequency harmonics of the grid current, whose parameters are shown in Table VI. Two power analyzers are used to measure the input and output power.

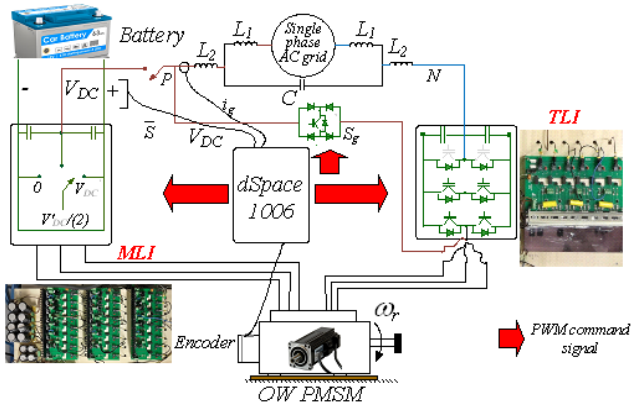

Fig. 23: Experimental test bench

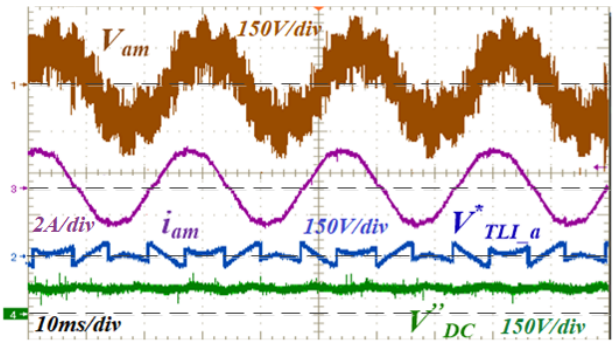

Fig. 24 TM: V_m, i_m, V_m* and V_{DC}''.

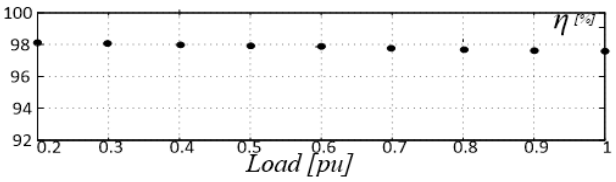

Fig. 25 TM: Converter efficiency vs. load at rated speed.

This work is licensed under a Creative Commons Attribution 4.0 License. For more information, see https://creativecommons.org/licenses/by/4.0/

This article has been accepted for publication in a future issue of this journal, but has not been fully edited. Content may change prior to final publication. Citation information: DOI 10.1109/OJIA.2020.3035851, IEEE Open Journal of Industry Applications

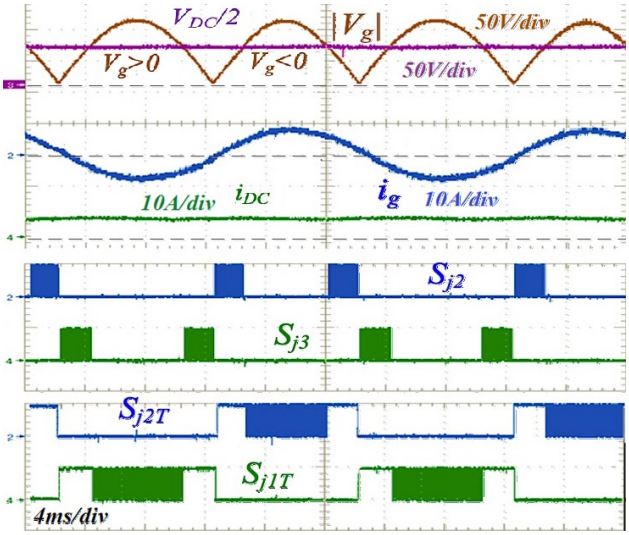

Fig. 26: G2V ac-dc (S_g *off*, V_{DC}=*55V*, i_{DC}=*6A*, V_{gpk}=*110V*, i_{gpk}=*6A*, P_{DC}=*330W*, P_{AC}=*360W*): grid voltage V_g, battery voltage V_{DC}, grid current i_g, battery current i_{DC}, and gate signals.

Motor phase voltage in traction mode is shown in Fig. 24 (ω_r =*80rad/s*, *50%* rated torque, V_{DC}'=*300V*, V_{DC}''=*50V*). The converter efficiency at rated speed is shown in Fig. 25 as function of the torque load. An exhaustive evaluation of the performance of the AHMC in ac motor drive applications can be found in [22]. Fig. 26 deals with ac single phase G2V operation at i_{DC}^*=*6A*. The grid current is in phase with the grid voltage and its waveform is very close to a sinusoidal one, leading to a 1.2% THD and a high power factor.

The performance of the control system in managing the battery current is quite satisfactory, as shown in Fig. 27, dealing with the response to a step variation of the reference current.

Ac single phase V2G operations are described in Figs. 28 and 29. More precisely, Fig. 28 deals with steady state operation at i_g=*6A*. An almost perfectly sinusoidal current is delivered to the grid, in phase opposition with the grid voltage. The THD of the grid current is 1.3%. A quick response of the system to a step variation of the reference grid current is shown in Fig. 29.

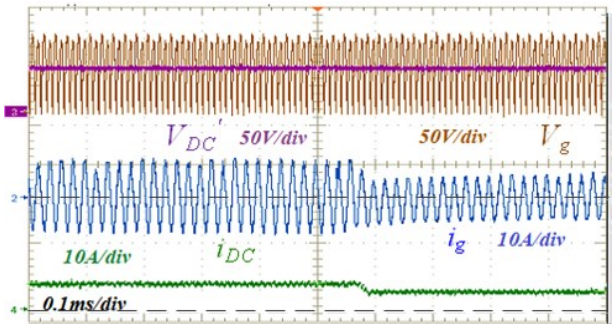

Fig. 27: G2V ac-dc - Battery current step variation from *1* to *0.6 p.u.* Grid voltage V_g, battery voltage V_{DC}, grid current i_g and battery current i_{DC}.

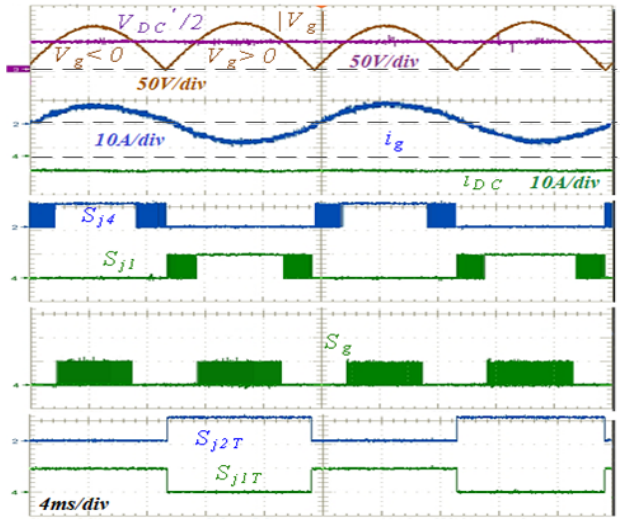

Fig. 28. V2G ac-dc - steady state (V_{DC}=*55V*, i_{DC}=*4.7A*, V_{gpk}=*110V*, i_{gpk}=*5A*, P_{DC}=*250W*, P_{AC}=*275W*): grid voltage V_g, battery voltage, grid current i_g, battery current i_{DC}, and gate signals.

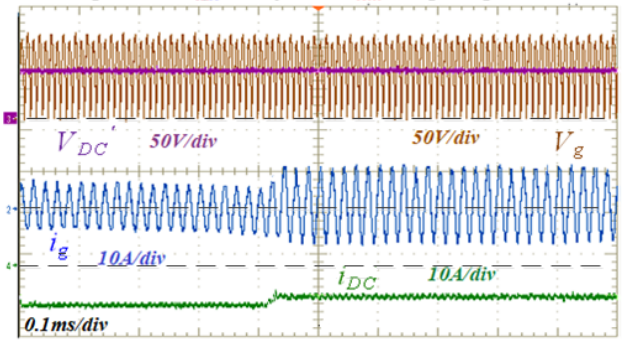

Fig. 29: V2G ac-dc - Battery current step variation from *1* to *0.6 p.u.*: Grid voltage V_g, battery voltage V_{DC}, grid current i_g and battery current i_{DC}.

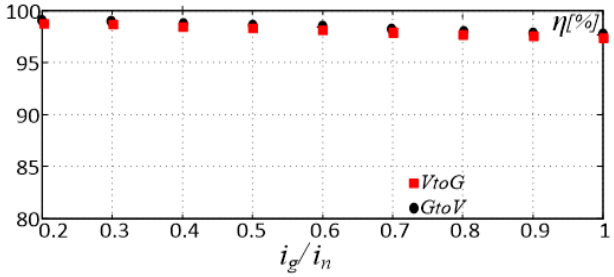

Fig. 30: Converter efficiency.

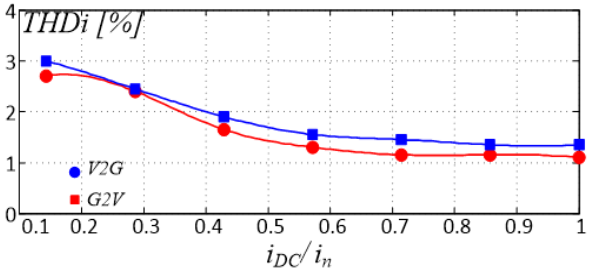

Fig. 31: Grid current THD.

This work is licensed under a Creative Commons Attribution 4.0 License. For more information, see https://creativecommons.org/licenses/by/4.0/

This article has been accepted for publication in a future issue of this journal, but has not been fully edited. Content may change prior to final publication. Citation information: DOI 10.1109/OJIA.2020.3035851, IEEE Open Journal of Industry Applications

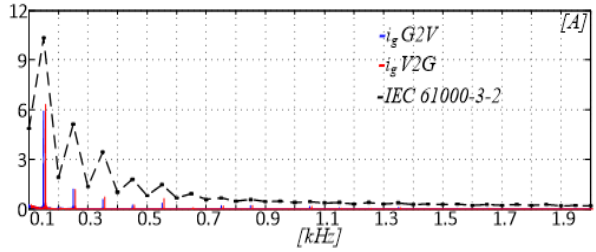

Fig. 32: G2V and V2G ac-dc: grid current harmonic spectrum and IEC 61000-3-2 compliance mask.

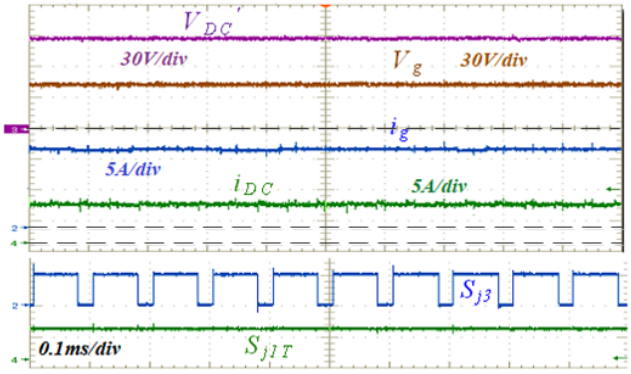

Fig. 33: G2V dc-dc - steady state. $V_g<V_{DC}$ (V_{DC}=55V, i_{DC}=6A, V_{gpk}=30V, i_{gpk}=12A, P_{DC}=330W, P_{AC}=360W): grid voltage V_g, battery voltage V_{DC}, grid current i_g, battery current i_{DC} and gate signals.

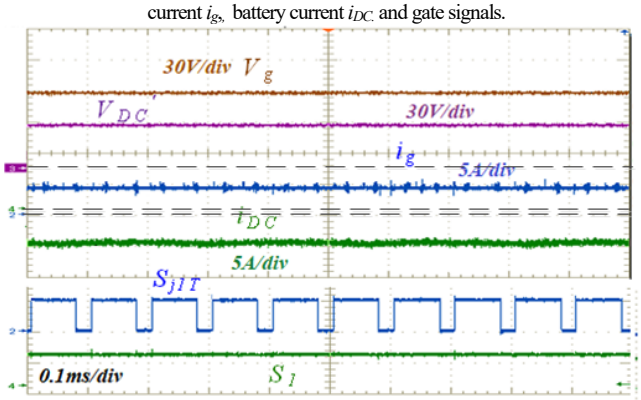

Fig. 34: G2V dc-dc - steady state. $V_g>V_{DC}$ (V_{DC}=45V, i_{DC}=6A, V_{gpk}=75V, i_{gpk}=4A, P_{DC}=270W, P_{AC}=300W): grid voltage V_g, battery voltage V_{DC}, grid current i_g, battery current i_{DC} and gate signals.

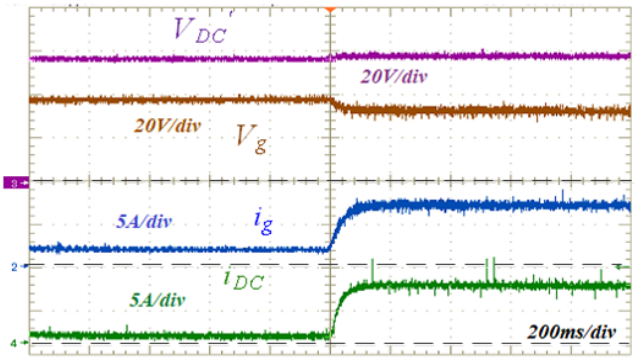

Fig. 35: G2V dc-dc - Battery current step variation from *0.2* to *1p.u.* (V_{DC}=55V, i_{DC}=2A, V_{gpk}=40V, i_{gpk}=3A) (up): grid voltage V_g, battery voltage V_{DC}, grid current i_g and, battery current i_{DC}.

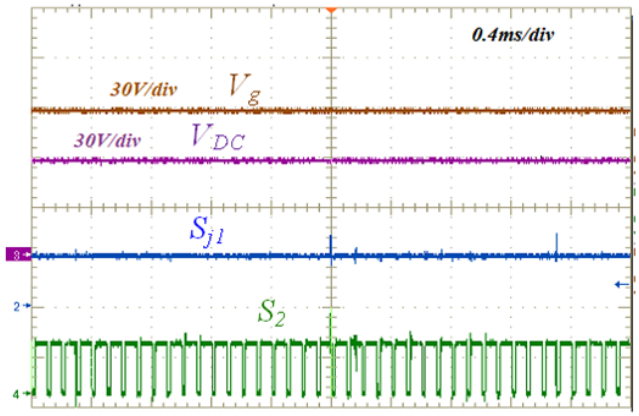

Fig. 36: V2G dc-dc - steady state: grid voltage V_g, battery voltage V_{DC}, grid current i_g, battery current i_{DC} and gate signals.

A good conversion efficiency η is achieved either in G2V either in V2G operation, as shown in Fig. 30. Moreover, a quite low grid current THD has been obtained in both modes, as shown in Fig. 31. The compliance of the experimental system with IEC 61000-3-2 standard was positively assessed. G2V dc-dc operations for $V_g<V_{DC}$ (Boost mode) and $V_g>V_{DC}$ (Buck mode) are shown respectively in Figs 33 and 35, while the response to a battery current step variation is shown in Fig. 35. Figures 36 and 37 respectively deal with steady state V2G dc-dc operation and with a step variation of the reference grid current. The total conversion efficiency η in dc-dc mode has been finally assessed for both G2V and V2G modes, as shown in Fig. 38.

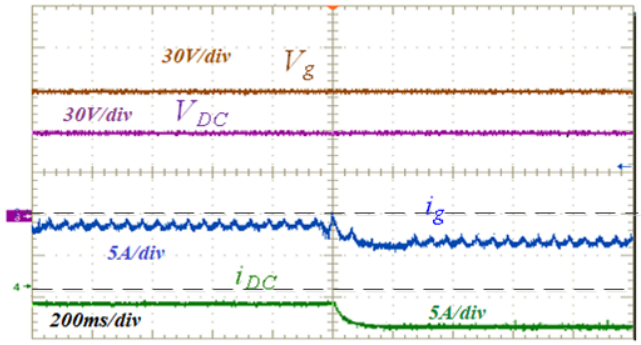

Fig. 37: V2G dc-dc - Battery current step variation from *0.2* to *1p.u.* (V_{DC}=60V, i_{DC}=5.5A, V_{gpk}=90V, i_{gpk}=4A, P_{DC}=330W, P_{AC}=360W): grid voltage V_g, battery voltage V_{DC}, grid current i_g and battery current i_{DC}.

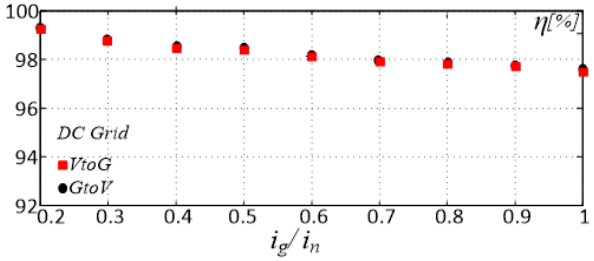

Fig. 38: Converter efficiency for dc-dc G2V and V2G.

Table V – PMSM technical data

P_n	L_s	V_n	R_s	i_n	λ_{PM}	ω_r	pp
2 kW	30 mH	380 V	4.3 Ω	6.1 A	0.17 Wb	2 krpm	3

Table VI – LCL filter technical data.

L_1	C	L_2
300 μH	2.2 μH	150 μH

This work is licensed under a Creative Commons Attribution 4.0 License. For more information, see https://creativecommons.org/licenses/by/4.0/

This article has been accepted for publication in a future issue of this journal, but has not been fully edited. Content may change prior to final publication. Citation information: DOI 10.1109/OJIA.2020.3035851, IEEE Open Journal of Industry Applications

VI. CONCLUSIONS

A way to obtain an integrated battery charger has been presented exploiting the Asymmetrical Hybrid Multilevel Converter topology. The transition from the traction configuration to the charger one can is accomplished only by acting on the control system, no additional electro-mechanical switches being required. Moreover, by introducing a single extra power switch a bilateral power flow can be managed enabling vehicle to grid operations. Such a power switch will become likely unnecessary o next generation EV equipped with battery packs featuring up to *800V*. The obtained integrated battery charger can be connected for V2G operations either to a standard ac single-phase grid, either to a dc power source for direct exploitation of domestic energy resources. On one side the proposed approach is valuable as it gives noticeable further features to an electric motor drive configuration that has proved to be more efficient than conventional two-level and multilevel systems. On the other side it allows to realize an on-board battery charger with a negligible impact on the vehicle range, available internal space and maximum payload.

REFERENCES

[1] D. Patil, V. Agarwal, "Compact Onboard Single-Phase EV Battery Charger With Novel Low-Frequency Ripple Compensator and Optimum Filter Design" IEEE Trans. on Vehicular Technology, Vol. 65, No. 4, pp. 1948-1956, 2016.

[2] H. Chen, X. Wang, and A. Khaligh, "A single stage integrated bidirectional AC/DC and DC/DC converter for plug-in hybrid electric vehicles," in Proc. IEEE Veh. Power Propulsion Conf., Sep. 2011, pp. 1–6.

[3] R. Nelson and M. Kepros, "AC ripple effects on VRLA batteries in float applications," Proc. 14th Annu. Battery Conf. Appl. Adv., 1999, pp. 281–289.

[4] A. Harrison, "Batteries andac phenomena in UPS systems: The battery point of view," in Proc. IEEE Telecommun. Energy Conf., Oct. 1989, vol.1, pp. 12.5/1–12.5/6.

[5] I. Subotic, N. Bodo, E. Levi, "Single-Phase On-Board Integrated Battery Chargers for EVs Based on Multiphase Machines" IEEE Trans. on Power Elect., Vol. 31, No. 9, pp. 6511-6523, 2016.

[6] Ivan Subotic, Emil Levi A, "Review of Single-Phase On-Board Integrated Battery Charging Topologies for Electric Vehicles" Proc. IEEE Workshop on Electrical Machines Design, Control and Diagnosis (WEMDCD), pp. 136-145, 2015.

[7] L. Solero, "Nonconventional on-board charger for electric vehicle propulsion batteries," IEEE Trans. on Vehicular Technology, vol. 50, no. 1, pp. 144-149, 2001.

[8] A. Testa, S. De Caro, T. Scimone, S. Panarello "A Buck-Boost based DC/AC Converter for Residential PV Applications" 21st International Symposium on Power Electronics, Electrical Drives, Automation and Motion (SPEEDAM 2012). Sorrento, Italy, June, 20-22, p. 114-119.

[9] A. Testa, S. De Caro, T. Scimone "Analysis of a VRB energy storage system for a tidal turbine generator" 13th European Conference on Power Electronics and Applications (EPE '09) p. 5798-5807, Barcelona, Spain, 8-10 Sept.

[10] M. Yilmaz and P. Krein, "Review of battery charger topologies, charging power levels, and infrastructure for plug-in electric and hybrid vehicles," IEEE Trans. Power Electron., vol. 28, no. 5, pp. 2151–2169, May 2013.

[11] A. Khaligh and S. Dusmez, "Comprehensive topological analysis of conductive and inductive charging solutions for plug-in electric vehicles," IEEE Trans. Veh. Technol., vol. 61, no. 8, pp. 3475–3489, Oct. 2012.

[12] D. O'Sullivan et al., "Power-factor-corrected single-stage inductive charger for electric-vehicle batteries," in Proc. IEEE 31st Annu. Power Electron. Spec. Conf., 2000, vol. 1, pp. 509–516.

[13]] H. Chen, X. Wang, and A. Khaligh, "A single stage integrated bidirectional AC/DC and DC/DC converter for plug-in hybrid electric vehicles," in Proc. IEEE Veh. Power Propulsion Conf., Sep. 2011, pp. 1–6.

[14] R. Nelson and M. Kepros, "AC ripple effects on VRLA batteries in float applications," in Proc. 14th Annu. Battery Conf. Appl. Adv., 1999, pp. 281–

[15] J. M. Slicker, "Pulse width modulation inverter with battery charger" Patent US 4,491,768, 1985.

[16] J. Y. Lee, H. S. Song, I. P. Yoo, K. Y. Jang, S. Shin, J. H. Joo,"System for recharging plug-in hybrid vehicle and control method for the same" Patent US 20120049803 A1, 2012.

[17] S. D'Arco, L. Piegari, M. S. Quraan, P. Tricoli, "Battery charging for electric vehicles with modular multilevel traction drives" Proc. IET Int. Conf. on Power Electronics, Machines and Drives PEMD, 2014.

[18] M. Marzouk, J. P. Ferrieux, D. Frey, B. Sarrazin, "A shared traction drive and battery charger modes for plug-in hybrid electric vehicle application" Proc. European Conf. Power Electronics and Applications EPE, 2014.

[19] J. Hong, H. Lee, K. Nam, "Charging method for the secondary battery in dual-inverter drive systems for electric vehicles" IEEE Trans. on Power Electronics, vol. 30, no. 2, pp. 909-921, 2015.

[20] M. Yilmaz and P. T. Krein, "Review of the Impact of Vehicle-to-GridTechnologies on Distribution Systems and Utility Interfaces," IEEE Trans. Power Electron., Vol.28, No.12, pp. 5673-5689, Dec. 2013

[21] S. Foti, A, Testa, G. Scelba, S. De Caro, M. Cacciato, G. Scarcella and Tommaso Scimone, "An Open-End Winding Motor Approach to Mitigate the Phase Voltage Distortion on Multilevel Inverters" IEEE Trans. Power Electronics, vol. 33, no. 3, pp. 2404-2416, March 2018.

[22] S. Foti, S. De Caro, G. Scelba, T. Scimone, A. Testa, M. Cacciato, G. Scarcella, " An Optimal Current Control Strategy for Asymmetrical Hybrid Multilevel Inverters" IEEE Trans. Ind. Appl., vol. 54, no. 5, pp. 4425-4436, Oct. 2018.

[23] S. Foti, G. Scelba, A. Testa, A. Sciacca, " An Averaged-Value Model of an Asymmetrical Hybrid Multi-Level Rectifier" Energies 2019, 12, 589.

[24] S. Foti, A. Testa, S. De Caro, T. Scimone, G. Scelba, G. Scarcella, " An open-end winding approach to the design of multi-level multi-motor drives" in Proc. of IECON 2016, Florence , Italy, Pages 5026-5032.

[25] S. Foti, A. Testa, G. Scelba, V. Sabatini, A. Lidozzi, L. Solero, "Asymmetrical hybrid unidirectional T-type rectifier for high-speed gen-set applications," proc. of IEEE Energy Conversion Congress and Exposition (ECCE), 2017, pp. 4887-4893.

[26] S. Foti, S. De Caro, G. Scelba, T. Scimone, A. Testa, G. Scarcella, "Multi-level open end windings multi-motor drives", Energies, Volume 12, Issue 5, 5 March 2019, Article number 861.

[27] S. De Caro, S. Foti, G. Scelba, T. Scimone, A. Testa, " A six-level asymmetrical Hybrid Photovoltaic Inverter with inner MPPT capability" Proc. IEEE 6th International Conference on Clean Electrical Power (ICCEP), pp. 631-635, 2017.

[28] Electric Vehicle and Plug in Hybrid Electric Vehicle Conductive Charger Coupler, SAE International, Standard Recommended Practice J1772, Jan. 2010

[29] F. Locment, M. Sechilariu, "Modeling and Simulation of DC Microgrids for Electric Vehicle Charging Stations" Energies 2015, 8, pp. 4335-4356.

[30] B. Arbetter, R. Erickson and D. Maksimovic, "DC-DC converter design for battery-operated systems," Proceedings of PESC '95 - Power Electronics Specialist Conference, Atlanta, GA, USA, 1995, pp. 103-109 vol.1.

[31] S. Foti, A. Testa, G. Scelba, V. Sabatini, A. Lidozzi and L. Solero, "A Low THD Three-Level Rectifier For Gen-Set Applications," in IEEE Transactions on Industry Applications, vol. 55, no. 6, pp. 6150-6160, Nov.-Dec. 2019.

This work is licensed under a Creative Commons Attribution 4.0 License. For more information, see https://creativecommons.org/licenses/by/4.0/